Materials Transactions, Vol. 49, No. 11 (2008) pp. 2702 to 2708

Effects of Welding Parameters on the Mechanical Performance of Laser Welded Nitinol

M. I. Khan*, S. K. Panda and Y. Zhou

Department of Mechanical Engineering, University of Waterloo, Waterloo, Ontario, Canada

The excellent pseudoelasticity, shape memory and biocompatibility of Nitinol has made it a leading candidate for various applications, including aerospace, micro-electronics and medical devices. Challenges associated with the welding Nitinol need to be resolved before its full potential in practical applications can be attained. The current study details the effects of process parameters on the mechanical and pseudoelastic properties of Ni-rich pulsed Nd:YAG laser welded Nitinol. The weld strength, pseudoelastic and cyclic loading properties for varying welding parameters are compared to those of the base metal. Furthermore, fracture surfaces have been analysed and detailed. Results show that process parameters greatly influence the mechanical performance and fracture mode of weldments.
[doi:10.2320/matertrans.MRA2008243]

(Received July 31, 2008; Accepted August 22, 2008; Published October 16, 2008)

Keywords: *laser micro-welding (LMW), nitinol, mechanical properties, pseudoelasticity, cyclic loading, fracture surfaces*

1. Introduction

The shape memory and pseudoelastic properties of Nitinol have shown promising solutions for problems in various applications including aerospace, micro-electronics and medical devices.[1–3] Laser welding is widely used during the fabrication of all of the aforementioned applications. Comprehensive research on the base metal properties of various NiTi alloys continues to be conducted.[4] However, challenges faced with welding have yet to be resolved before the safe integration of this material can progress in many of these applications.

To date, only limited literature exists detailing the mechanical properties of laser welded Nitinol sheet. Earlier studies by Schloßmacher *et al.* investigated laser welding of Ni-rich and Ti-rich Nitinol.[5,6] Ti-rich alloys showed reduced mechanical performance, which was attributed to Ti_2Ni intermetallic (IMC) formation in weld metal. In contrast, the Ni-rich alloys were found to retain pseudo-elastic properties and the formation of Ni_4Ti_2 IMC was observed within the welds. In addition, Schüßler showed nominal changes compared to base material during high cycle fatigue at low strain for Ni-rich Nitinol.[7] Tuissi *et al.* investigated the functional properties of Ni-rich Nitinol and stated a decrease in pseudoelastic properties, contrary to the work presented by Schloßmacher *et al.*[8] Hsu *et al.* isolated and tested the weld material for equiatomic and Ni-rich Nitinol.[9] It was shown that the equiatomic weld metal exhibited higher strength when compared to base metal. Furthermore, cyclic loading results for the Ni-rich Nitinol showed increased permanent residual strain for the weld metal. More recently, Falvo *et al.* showed that large strain applications of Ti-rich Nitinol should be avoided and stated a need to further investigate the effects of process parameters.[10] A technical appraisal of shape memory alloys conducted by Chau *et al.* reiterated that much more research still needs to be undertaken before practical applications can commence.[11]

It is well known that welding parameters can greatly influence the mechanical properties of laser welded materials. As acknowledged in recent publications, the influence of laser welding process parameters, including pulse frequency and peak power, on the mechanical properties of Nitinol have yet to be detailed.[10,11] The objectives of the current study are to detail the effects of process parameters on the mechanical and pseudoelastic properties of Ni-rich laser welded NiTi alloy.

*Corresponding author, E-mail: Ibraheem@rogers.com

2. Experimental Methods and Conditions

2.1 Material

Commercially available SE508 Nitinol strip 0.37 mm thick was used in this study. The chemistry for this particular alloy was 55.8 mass% Ni and 44.2 mass% Ti with maximum oxygen and carbon contents of 0.05 mass% and 0.02 mass%, respectively. The as-received cold-rolled material was heat treated for 1 hour at 800°C to attain pseudoelastic properties. A dilute solution of hydrofluoric and nitric acid was used to remove the black oxide before laser welding.

Base metal DSC analysis was conducted using a Thermal Analysis Q2000 system equipped with a refrigerated cooling system (RCS). DSC curves were recorded in a temperature range from −50°C to 40°C under a controlled heating and cooling rate of 5°C/min. The DSC curve detailing transformation temperatures for the base material is shown in Fig. 1. Both austenite finish (A_f) and martensite start (M_s) temperature were below room temperature, −8.61°C and −33.27°C, respectively. This indicates room temperature phases are predominantly austenite, therefore pseudoelastic behaviour should be present during tensile testing.

2.2 Welding equipment and parameters

Laser welds were produced using a Myachi Unitek pulsed Nd:YAG (neodymium-doped yttrium garnet) laser welder (Model LW50 A) which produces a beam with a 1.06 μm wavelength. This particular system is equipped with a power monitor allowing for accurate insitu assessment of welding power. Welds were conducted on monolithic sheets. Top and bottom shielding of argon was implemented to minimize oxidation; a flow rate of 30 CFH was selected, as per a previous study on titanium alloys.[12]

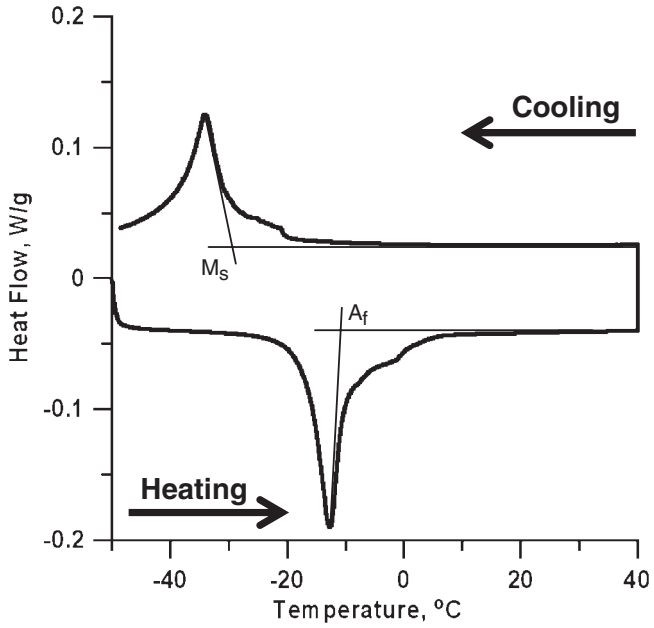

Fig. 1 DSC curve for base-metal NiTi alloy.

Table 1 Selected welding parameters.

Welding condition (peak power, frequency)	*Welding speed*
0.6 kW, 10 pps	48.0 mm/min
0.7 kW, 10 pps	48.0 mm/min
0.8 kW, 10 pps	48.0 mm/min
0.9 kW, 10 pps	48.0 mm/min
0.6 kW, 1 pps	4.80 mm/min
0.6 kW, 5 pps	24.0 mm/min
0.6 kW, 15 pps	72.0 mm/min

Welds were produced using a 400 µm spot diameter and 3 ms pulse time. Minimum weld criteria included full penetration and hermetic seal conditions. It was determined that 0.6 kW peak pulse power was sufficient for producing full penetration welds. References have shown that 80% overlap of melted spots will produce hermetic welds.[13] Table 1 shows the selected welding parameters, variable process parameters included pulse frequency and peak power. Welding parameters were selected using eq. 1, which correlates the various welding parameters including frequency (f), spot diameter (d_s), welding speed (V) and percent overlap (%OL).

$$f = 100V/(d_s)(100\text{-}\%\text{OL}) \quad (1)$$

From the above equation it can be shown that the pulse frequency and welding speed are directly related (i.e. higher pulse frequency leads to higher welding speed). Hence the terminology welding speed (V) will be referred to as pulse frequency (f).

2.3 Mechanical testing

Tensile specimens were prepared using wire EDM cutting in order to minimize effects of burrs during mechanical deformation. A transverse weld configuration was selected to investigate the effects of both weld and base metal. Figure 2 shows a schematic of the tensile specimen with dimensions; the sub-sized samples were selected to have sufficient weld area along the gauge length. Tests were performed using an Instron model 5548 micro tensile machine with a load cell resolution of ±3 N. All tests were performed at room temperature (25°C). Cyclic loading was conducted using a cross head speed of 0.04 mm/min to apply a first loading cycle up to a strain of 0.06 mm/mm followed by an unloading cycle down to a stress of 7 MPa. The same cycle was repeated 50 times (50 cycles) for both parent and laser welded specimens. After completion of 50 cycles the specimens were strained at a cross head speed of 0.4 mm/min until fracture.

Figure 3 a shows a typical stress-strain curve for the base metal consisted of three distinct deformation zones: elastic (region 1), pseudo-elastic (region 2) and plastic deformation (region 3). During cyclic loading the maximum strain (0.06 mm/mm) remains within the pseudoelastic region. A schematic of the stress strain curve of a loading-unloading cycle for a typical NiTi exhibiting pseudoelastic behaviour is shown in Fig. 3(b). It is well known that the pseudoelastic characteristic of Nitinol makes it an excellent material for energy storage.[14] The pseudoelastic parameters E_1, E_2 and permanent residual strain are defined in this figure. E_1 is the energy dissipated per unit volume in one complete cycle and E_2 is the stored energy per unit volume on loading and available for release during unloading. The efficiency for energy storage (η), defined by Lin and Wu,[15] is expressed in eq. 2.

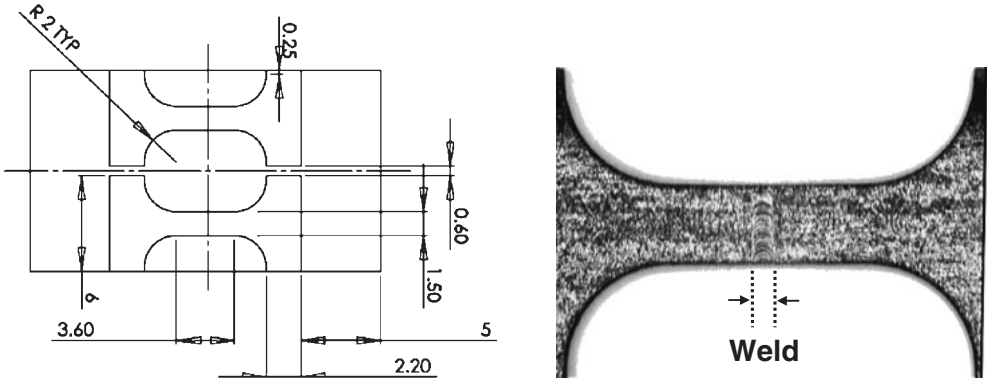

Fig. 2 Schematic showing dimensions of tensile coupons.

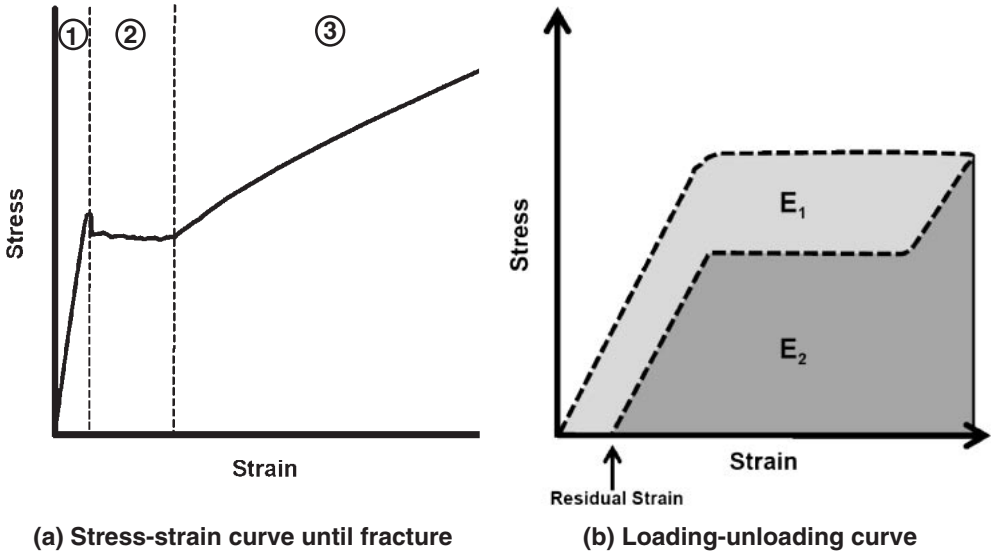

Fig. 3 Schematic of a typical stress-strain curve for pseudoelastic NiTi alloy.

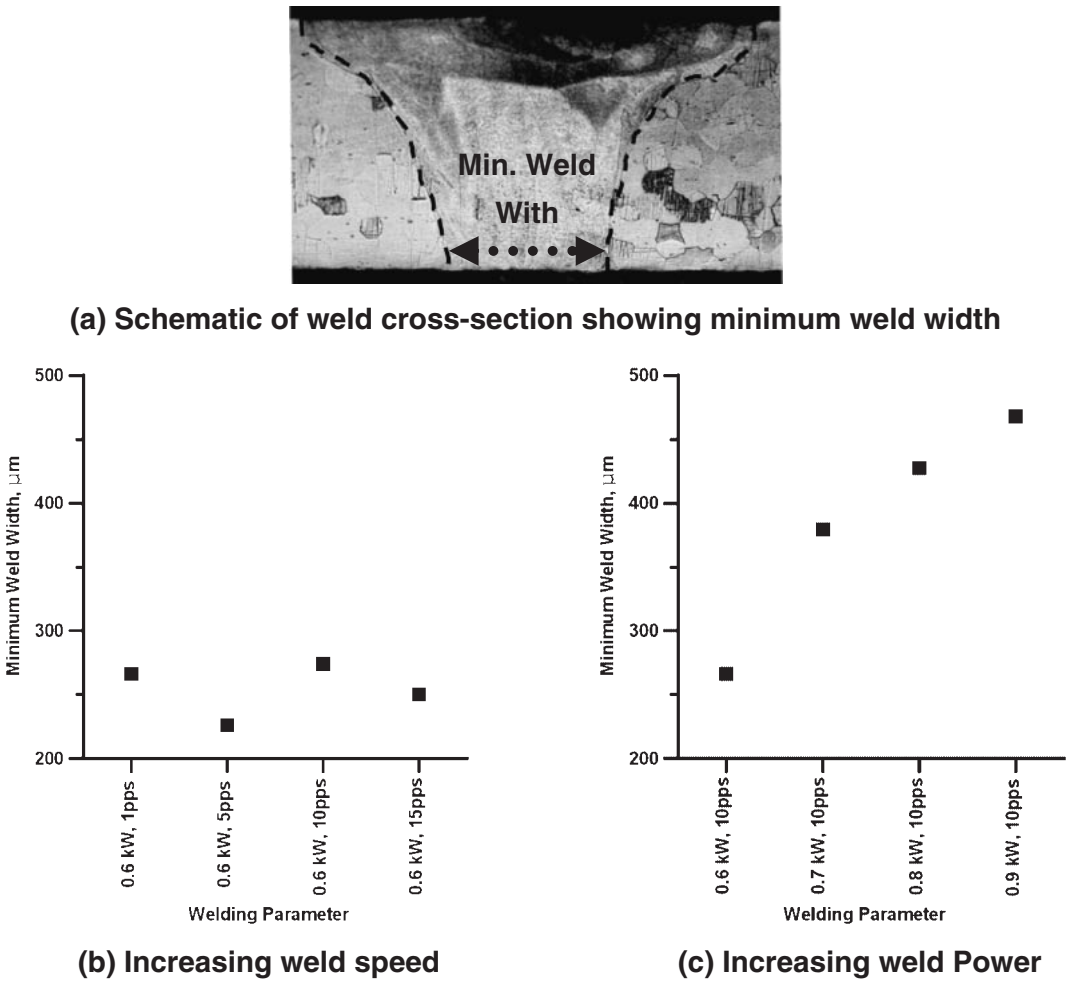

Fig. 4 Effect of process parameters on weld width.

$$\eta = E_2/(E_2 + E_1) \tag{2}$$

The dimensions of the welds were measured using metallographic procedures. Mounted samples were ground using SiC paper with successively decreasing grit size. Samples were polished using 1 µm diamond and etched with 14 mL HNO_3, 3 mL HF and 82 mL H_2O. Figure 4 shows the effect of pulse frequency and peak power on the minimum weld width. Minimum weld width is depicted in the schematic shown in Fig. 4(a). Nominal change to the weld width was observed with increasing pulse frequency while maintaining weld power, as shown in Fig. 4(b). However with increasing weld

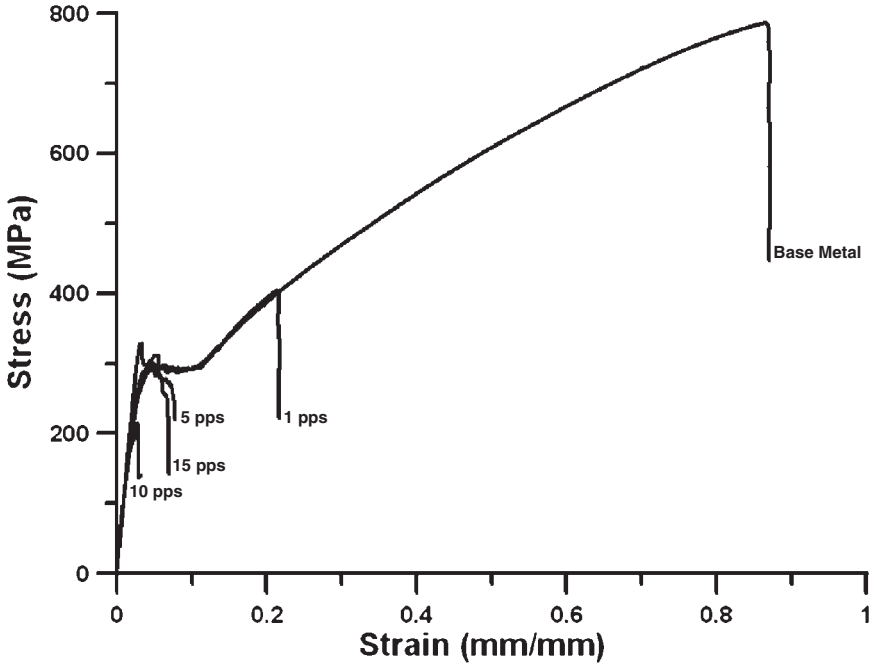

Fig. 5 Representative tensile curves for varying pulse frequency for 0.6 kW power.

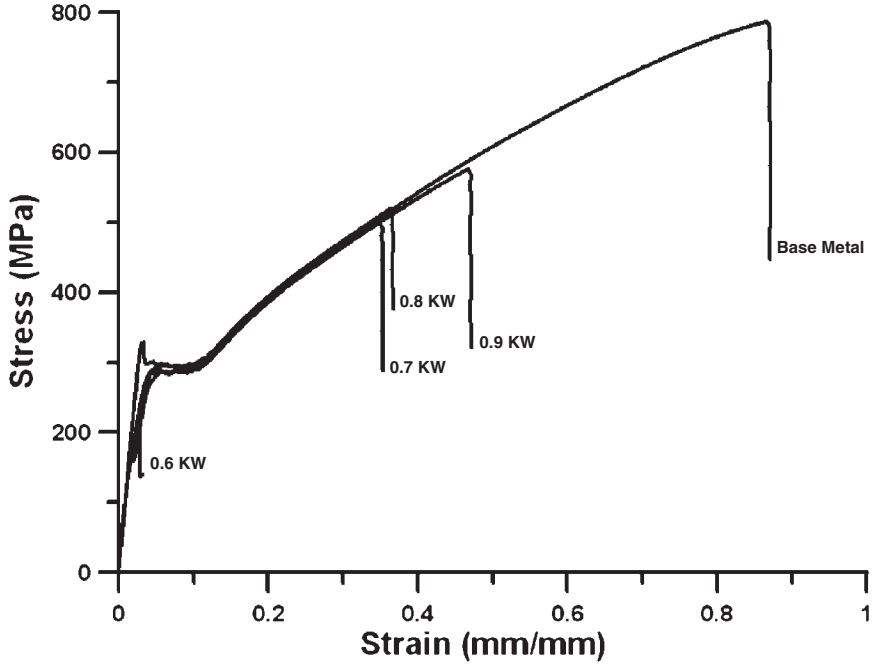

Fig. 6 Representative tensile curves for varying peak power input for 10 pps frequency.

power the minimum weld width increased from 260 µm to 460 µm with power increasing from 0.6 to 0.9 kW.

3. Results and Discussion

3.1 Stress strain curves

Comparisons between engineering stress-strain curves for unwelded and welded specimens of varying pulse frequency and power input are shown in Fig. 5 and Fig. 6 respectively. Typical pseudo-elastic behaviour of shape memory alloys was observed for the base metal specimen, indicated by a flat region (plateau) after linear elastic straining near 0.03 mm/mm strain and 290 MPa stress. Beyond 0.12 mm/mm strain, plastic deformation of martensite occurred and the load increased due to strain hardening, followed by failure near 0.90 mm/mm strain.

Figure 5 shows that the ductility and strength decreased significantly for the 0.6 kW laser welded specimen with higher pulse frequency (5 pps, 10 pps and 15 pps). This was due to premature failure in the weld zone before sufficient stress could be applied to transform the adjacent base metal to martensite. However, a slight increase in ductility and strength was observed at the lowest pulse frequency of 1 pps in the 0.6 kW laser weld (Fig. 5). The 1 pps weldment was

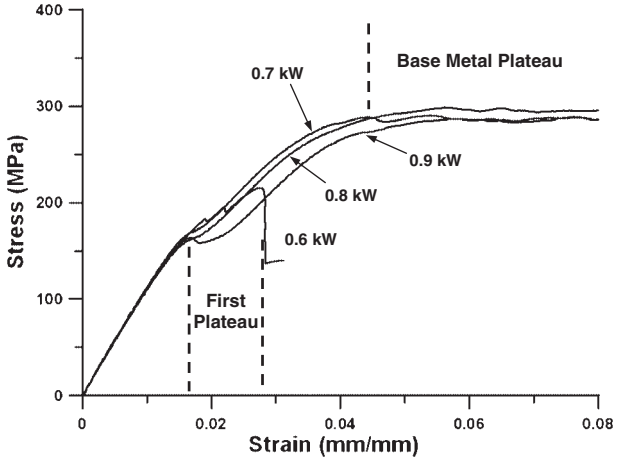

Fig. 7 Detailed view of multiple plateaus in welded samples.

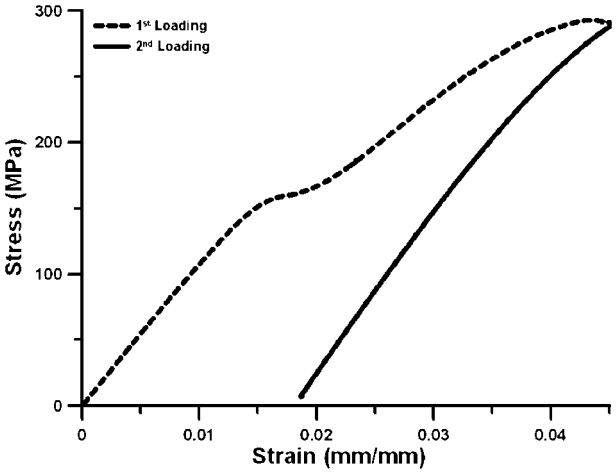

Fig. 8 First and second loading curves for 0.9 kW, 10 pps weld.

also able to reach strains capable of inducing plastic deformation of martensite along the gauge length. The engineering stress-strain curves for varying welding conditions-peak power (0.6, 0.7, 0.8 and 0.9 kW) with constant pulse frequency (10 pps), are shown in Fig. 6. Except for the 0.6 kW weld, each of the other conditions (0.7, 0.8 and 0.9 kW) surpassed the pseudo-elastic region. However the failure strength and ductility of all welded specimens were less than 70% and 50% of those of the base metal, respectively. The effects of welding parameters showed an increase in tensile strength with increasing weld power. Previous studies have shown similar reduction of fracture strain of laser welded NiTi alloys.[5,7,9,10,16] This reduction has been attributed to several factors including segregation of solute during solidification and the coarse-grain and dendritic structure in the weld metal. However current results show that welding parameters can influence the mechanical properties; specifically, the higher energy input and lowered pulse frequency resulted in improved mechanical performance.

3.2 Pseudo-elasticity

Figure 7 details the stress-strain diagrams from elastic to the onset of pseudo-elastic deformation for un-welded and laser welded specimens for different welding powers. Typical pseudo-elastic behaviour of NiTi due to stress induced martensite (SIM) transformation was observed during straining (B2 $\rightarrow$ B19′) for most tensile specimens.[4,17] However, results showed evidence of an initial plateau in the welded specimens which became more pronounced with increasing peak welding power. This suggests an additional SIM transformation in the weld zone during straining before the usual pseudoelastic behaviour of the base metal. During loading, the transverse weld tensile coupon induced stress in both the base and weld metal. Hence, multiple plateaus may result from two separate transformations from two different regions.

The initial SIM transformation plateau occurred in the weld metal, between 0.015 mm/mm and 0.022 mm/mm strain; additional straining then induced transformation in the remaining gauge length. The second SIM transformation is interpreted as reflecting the BM stress-strain curve. In 1997, Schüßler conducted tensile tests on entirely remelted test specimens (which consisted of a fully laser processed gauge length).[7] A lower plateau stress for SIM formation and lower strain hardening during plastic deformation were observed compared to the base metal. Similarly in Fig. 7 the initial plateau in welded specimens occurred at a lower stress, which suggests transformation occurred in the weld. The amplified definition of the first plateau with increasing peak power may be attributed to the increasing weld width, as observed in Fig. 4. Increasing weld power resulted in a larger minimum weld width. Accordingly, a larger weld area within the gauge length underwent the initial SIM transformation.

It is well known that SIM transformation is irreversible when sufficient additional stress is applied to induce plastic deformation of martensite.[17] In order to further detail the dual SIM transformation, a 2-cycle loading test was conducted. Figure 8 shows the first and second loading curves for the 0.9 kW, 10 pps weld condition, which was strained up to 0.06 mm/mm. During initial loading, SIM transformation of the weld metal occurred followed by stresses high enough to induce plastic deformation of martensite. The second loading cycle showed the absence of the initial plateau, indicating the occurrence of irreversible SIM transformation within the weld metal.

Nitinol SIM transformation properties can be strongly influenced by processing routes and techniques.[4,17] Remelting due to laser welding alters base metal microstructure, which for nitinol can result in the formation of dendrites or coarse grains and segregations at grain boundaries.[6–8] Furthermore, abnormal room temperature phase shifts in Nitinol due to laser welding have also been reported.[9] These modifications to the weld metal may attribute to its altered SIM transformation behaviour. However, more detailed microstructural analysis of weld metal is required in order to determine the key factors responsible for the initial SIM transformation.

3.3 Energy absorption and cyclic loading

The variation of efficiency for energy storage (η) and permanent residual strain with number of cycles (N) are plotted in Fig. 9. Cyclic loading was not conducted on the 0.6 kW power laser welded samples with 5 pps, 10 pps and

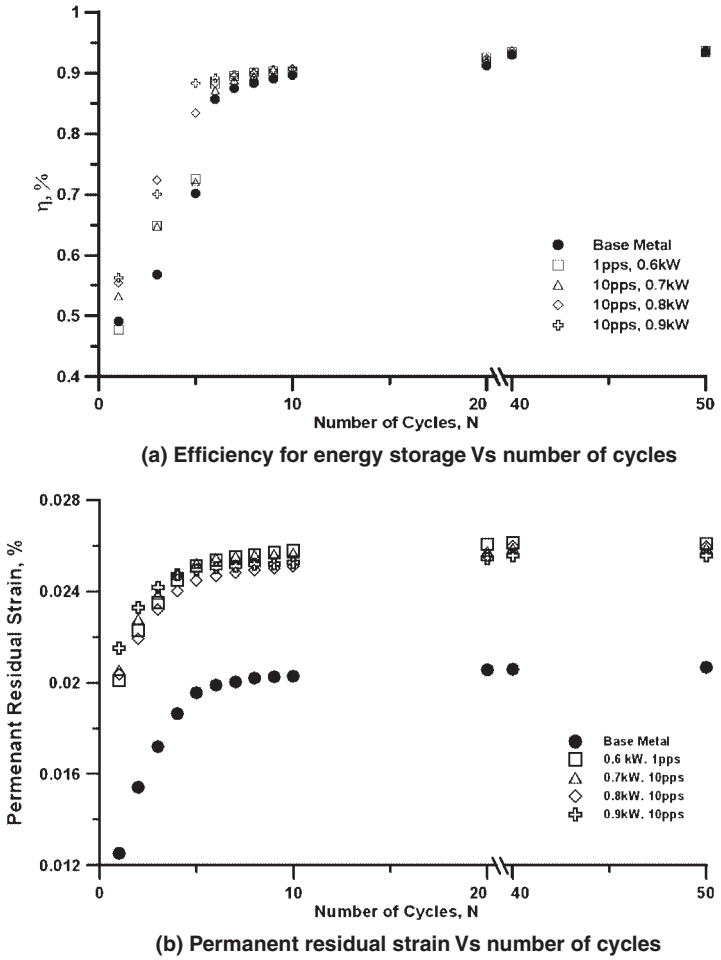

Fig. 9 Cyclic loading of unwelded and laser welded specimen up to 6% strain.

15 pps since premature failure occurred before 0.06 mm/mm strain. Figure 9(a) shows a rapid increase in permanent residual strain between 1 and 5 cycles for both base and weld metal. Beyond 5 cycles each material reached a steady state. The ability of a material to regain its original shape after unloading can be measured by permanent residual strain. All welded specimens showed higher permanent residual strain compared to the BM when straining up to 0.06 mm/mm. After 10 cycles the magnitudes of residual strain for base and weld metal were 0.020 and 0.026%, respectively. Figure 9(b) shows efficiency for energy storage (η) as a function of cycles (N). Both base and welded materials showed an increase in η up to 5 cycles. Weld material showed a slightly improved efficiency during the first 5 cycles. Beyond 20 cycles the efficiency stabilized near 0.9%. Hence compared to the base metal, welded coupons showed higher overall permanent residual strain and exhibited slightly higher efficiency for energy storage during the initial 5 cycles.

As detailed earlier, during the initial cycle SIM transformation occurred in the weld metal, resulting in a cold worked weld region. Therefore the increase in permanent residual strain of welded coupons could be due to the permanent SIM transformation after initial loading. In addition slight increase in permanent residual strain in the specimens made at higher power input can be attributed to the increased weld width. In 1994 Lin and Wu showed that improved η values can be attained by cold working TiNi SMA.[15] Hence the improved efficiency for the welded specimens during the initial cycles may be attributed to the plastic deformation of the weld metal after the initial cycle where SIM transformation is induced.

3.4 Fracture surfaces

Fracture surfaces for welded and unwelded tensile specimens are shown in Fig. 10. Failure occurred within the weld zone for each welded specimen. Base metal fracture surfaces, shown in Fig. 10(a), revealed a dimpled surface suggesting ductile fracture. Fig. 10(b) shows the fracture surface of the 0.6 kW and 1 pps weld condition, which exhibited lowest tensile strength. A smooth fracture surface showing the directional dendritic solidification structure of the weld was observed. This is indicative of transgranular failure where fracture propagates at the dendrite interface. In contrast, the 0.9 kW, 10 pps welding condition, shown in Fig. 10(c), revealed a relatively more coarse surface. When observed closely (Fig. 10(d)) a finer dimpled structure was exposed, suggesting ductile intergranular failure through the fusion zone dendrites. These results reveal that changing welding parameters can result in different failure modes; however, further research detailing weld microstructure is required to determine the mechanism responsible for this failure mode transition.

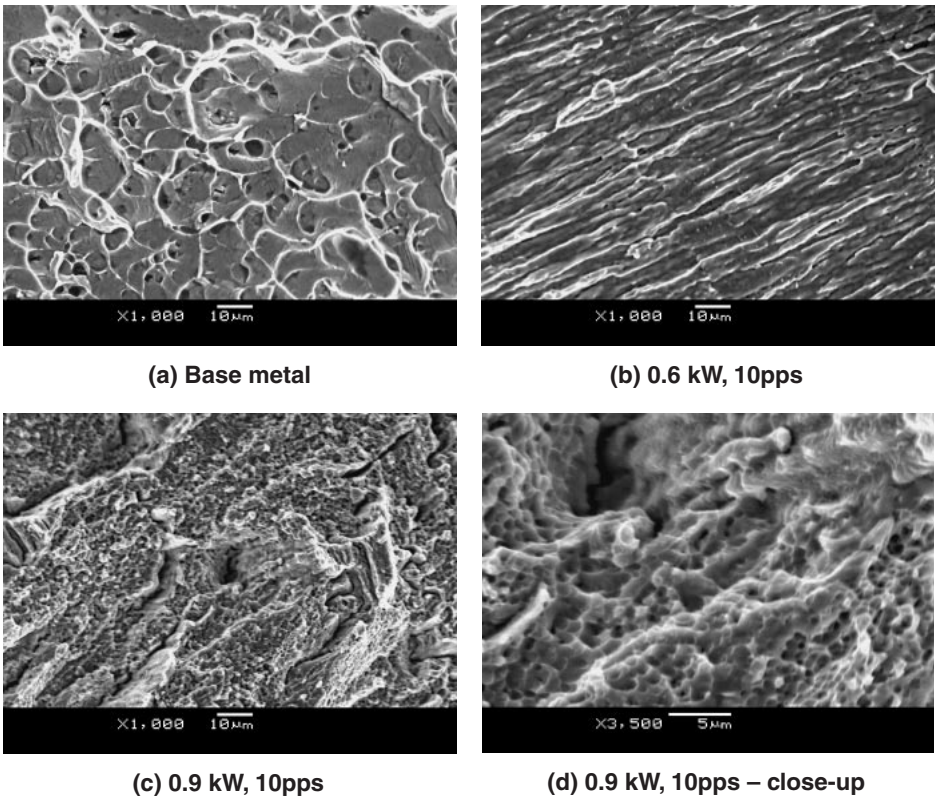

(a) Base metal (b) 0.6 kW, 10pps

(c) 0.9 kW, 10pps (d) 0.9 kW, 10pps – close-up

Fig. 10 Fracture surfaces of tensile specimens.

4. Conclusions

The current study investigated the mechanical properties of pulsed ND:YAG laser welded Nitinol. The weld strength, pseudoelastic and cyclic loading properties for varying welding parameters were compared with the base material and fracture surfaces were analysed.

Welding parameters (peak power and pulse frequency) were shown to strongly influence the mechanical properties (tensile strength and ductility) of the micro laser welded NiTi alloy. Higher peak power and lower pulse frequency resulted in improved mechanical performance. Evidence of multiple plateaus was observed in welded specimens during transverse tensile loading. These plateaus resulted from two separate SIM transformations during tensile deformation (weld and base metal). In addition, laser welded samples showed higher permanent residual strain and exhibited a slightly higher efficiency for energy storage during the initial 5 cycles compared to base material. Finally, fracture surfaces of base material revealed ductile dimpled surfaces while welded specimens exhibited both brittle (low peak power) and ductile (high peak power) failure modes.

Acknowledgement

The authors would like to acknowledge the support of the Natural Sciences and Engineering Research Council of Canada (www.nserc.ca) and the Canada Research Chairs Program (www.crc.gc.ca). The authors are also grateful to Andrew Wick of the Nitinol Device Company (NDC) for providing the material examined in this study.

REFERENCES

1) R. Pelton, D. Hodgson, S. Russell and T. W. Duerig: SMST-94 Proc. 1st Intl. Conf. On Shape Memory and Superelastic Technologies, A, (MIAS, Monterey, CA, 1994).
2) R. Pelton, D. Hodgson, S. Russell and T. W. Duerig: SMST-97 Proc. 2nd Intl. Conf. On Shape Memory and Superelastic Technologies, A, (MIAS, Monterey, CA, 1997).
3) S. Russell and R. Pelton: SMST-2000 Proc. 2nd Intl. Conf. On Shape Memory and Superelastic Technologies, A, (MIAS, Pacific Grove, CA, 2000).
4) K. Otsuka and X. Ren: Prog. Mater. Sci. **50** (2005) 511–678.
5) P. Schloßmacher, T. Haas and A. Schüßler: SMST-94, Proc. 1st Intl. Conf. On Shape Memory and Superelastic Technologies, ed. by A. R. Pelton, D. Hodgson, S. Russell and T. W. Duerig, (MIAS, Monterey, CA, 1994) pp. 85–90.
6) P. Schloßmacher, T. Haas and A. Schüßler: SMST-97, Proc. 2nd Intl. Conf. On Shape Memory and Superelastic Technologies, ed. by A. R. Pelton, D. Hodgson, S. Russell and T. W. Duerig, (MIAS, Monterey, CA, 1997) pp. 137–142.
7) A. Schüßler: SMST-97, Proc. 2nd Intl. Conf. On Shape Memory and Superelastic Technologies, ed. by A. R. Pelton, D. Hodgson, S. Russell and T. W. Duerig, (MIAS, Monterey, CA, 1997) pp. 143–148.
8) A. Tuissi, S. Besseghini, T. Ranucci, F. Squatrito and M. Pozzi: Mater. Sci. Eng. A **A273–275** (1999) 813–817.
9) Y. T. HSU, Y. R. Wang, S. K. Wu and C. Chen: Metall. Mater. Trans. A **32A** (2001) 569–576.
10) A. Falvo, F. M. Furgiuele and C. Maletta: Mater. Sci. Eng. A **412** (2005) 235–240.
11) E. T. F. Chau, C. M. Friend, D. M. Allen, J. Hora and J. R. Webster: Mater. Sci. Eng. A **438–440** (2006) 589–592.
12) X. Li, J. Xie and Y. Zhou: J. Mater. Sci. **40** (2005) 3437–3443.
13) P. W. Fuerschbach and D. A. Hinkley: Weld. J. **76** (1997) 103S–109S.
14) S. Miyazaki and K. Otsuka: ISIJ Inter. **29** (1989) 353–377.
15) H. C. Lin and S. K. Wu: Acta Metall. Mater. **42** (1994) 1623–1630.
16) Y. Ogata, M. Takatugu, T. Kunimasa, K. Uenishi and K. F. Kobayashi: Mater. Trans. **45** (2004) 1070–1076.
17) J. Van Humbeeck: Adv. Eng. Mater. **3** (2001) 837–850.